African Journal of Biological Sciences

Effect of ZnO on the spectroscopic, structural and physical properties of CaO-Sb₂O₃-B₂O₃ glasses for non-linear optical Applications

Rajesh Alukucha[a], Pallati Naresh[b], Jagram Anterbedy[a], Gangadhar Thalari[a]*

[a]*Department of Chemistry, University College of Science, Osmania University, Hyderabad-500007, Telangana ,India*

[a]*Department of Physics, University College of Science, Saifabad, Osmania University, Hyderabad-500007, Telangana ,India*

Corresponding Author: gangadharchemou@gmail.com

Abstract

A set of transparent glasses with chemical formula $xZnO+10CaO+10Sb_2O_3+(80-x)B_2O_3$ (x = 0 to 20 with 5mol% stepwise) were synthesized via melt-fast quench method. The basic non-crystallinity of present glasses was determined with X-Ray diffraction (XRD) measurement. An appearance of the broad humps in the XRD spectra is the characteristic nature of the non-crystalline materials. The density based physical aspects of the glasses were measured and determined by Archemeds method. It was found to increase with the incorporation of modifier ZnO. The optical features of the glasses were analyzed with UV spectra. The cut-off edge from UV-Spectra increased from 296nm to 374nm: Indirect band gap varied between 3.90eV to 3.23eV: direct band gap varied from 3.97eV to 3.32eV; The Urbach energy (ΔE) increased from 0.65eV to 0.90eV with an addition of ZnO content. The higher refractive index found for the present glasses ranged 2.10 to 2.30. The structural variations in the glass network were studied with the help of FT-IR & Raman studies. FT-IR results proved the existence of BO_3, BO_4, SbO_3, SbO_6, ZnO_4 units and cationic vibrations. The Raman studies revealed different vibrational modes in the glass network. The higher refractive index of the studied glasses indicates the suitability for NLO applications

Keywords: Density, cut-off wavelength, Refractive index, FT-IR, Raman studies

1. Introduction

Borate based glass materials are familiar for their wide utility in various fields due to their superior optical transparency, low-melting points, high photon energy, Good chemical resistance, higher thermal durability, and Refractive index [**1, 2**]. The basic structural units of borate glass are BO_3 and BO_4. The structural modifications have been take place, when alkaline earth oxides incorporated into it. Especially, the incorporation of CaO and Sb_2O_3 play a vital role in the glass [**3**]. There is a disruption of B-O bands and transformation of structural units from coordination number 3 to 4 can be seen. It leads to resulting in the non-bridging oxygen in the glass networks. ZnO is an environmental friendly oxide which familiar for its economic viability, non-toxic behaviour, and good optical band gap energy. ZnO incorporated borate-based glasses suitable for the in-vivo and in-vitro applications because of the presence of its Zn^{+2} ions [**4**]. The dual role of ZnO as network former and network modifier depends on its composition. The addition of ZnO into borate-based glass network enhances the refractive index and the uniformity of glass at room temperatures [**5**]. The antibacterial efficiency of the ZnO-Borate glasses also high when compare to the other oxide glasses [**6**]. ZnO also enhances the radiation shielding capacity of the materials.

Antimony oxide Sb_2O_3 acts as network modifier in the glassy materials in the form of trigonal pyramids (SbO_3) and octahedral (SbO_6). The addition of Sb_2O_3 into borate based glass matrix, disrupts the original structure and it leads to the excess of oxygens in the form of NBOs. It also enhances the polymerization, increases the compactness of the glass network. Antimony oxide also suitable element for radiation shielding, third order non-linear optical applications, opto electronic device applications because of its higher density and third order non-linear susceptibility [**7**]. The Sb_2O_3 incorporation into increases the glass transition temperature Tg due to increased cross-linkages and structural rigidification [**8-9**]. It can promote nucleation and crystallization in certain glass-forming systems when present even at low levels. Therefore, it can be concluded that the Sb_2O_3 incorporation into the borate base glass leads to the SbO_3 and SbO_6 structural units in the glass impacting polymerization, phase separation, and improving durability through increased connectivity and compactness. It also is an important intermediate glass modifier.

The role of CaO in the glass network is as network modifier which supports the rigidity of the glass network and also involve in the breakage of bonds between boron-oxygen along with linkages. It show good and well bio activity against various bacterial strains after a stipulated period. Adding CaO to the glassy network, there is creation of NBOs which leads to the reaction of Ca^{+2} ions with the bacterial membrane and kills the cells of bacteria [**10**]. In the recent days, the borate glasses containing metal oxides such as CaO, ZnO, Sb_2O_3, Ag_2O etc. widely using for multiple applications [**11, 12**]. The incorporation of the metal oxides, rare earth oxides and etc. into borate glassy matrices have given fruitful results for various applications point of view. Previous and recent reports [**13**] on glasses explains the role of metal oxides in the variation of physical, structural, antibacterial efficacy, optical and also other properties of the glass materials and their significance in various fields.

The aim of the current study is to examine the role of ZnO incorporation into borate glass consisting CaO and Sb_2O_3 and its consequences related to structure, density based physical parameters, variations in optical properties, enhancement of conductivity and their applications. The effect of remaining modifiers on the studies also have been investigated.

2. Experimental section

Metal oxide (ZnO) doped glasses with a chemical composition of x ZnO-(80-x)B_2O_3-10CaO-10Sb_2O_3 where x values lies from 0 to 20 mol% with 5 variation were synthesized through the conventional melt-quench route. AR grade chemicals Sb_2O_3, CaO (Merck), B_2O_3 (AR grade) and ZnO were taken for preparation of the glass samples. About 15 grams of oxides powder are taken in a crucible made of porcelain, and melted at ~1100-1150°C for 1hr. The powder was melted and formed liquid. The liquid in the crucible was agitated/swirled frequently for 1 hr to form a homogeneous liquid melt. The crucible with melt was emptied on a steel plate which is at 200°C and hard-pressed using another steel disc which is also at 200°C which resulted in the formation of glasses. The prepared glassy samples were annealed at around 200°C for 24 hours for removal of thermal stress and strain and also to avoid cracking of glass samples. The glass samples thus obtained were shown good transparency. The glass formation was confirmed with the transparency and uniformity. Further, the prepared glasses were dipped into paraffin oil to avoid hygroscopic behaviour.

The density behaviour of the studied glasses was measured using DONA digital balance with immersion liquid Xylene with an accuracy of ± 0.01 g/cm^3. For the amorphous behaviour confirmation, the XRD spectrum was recorded on X-Ray diffractometer at room temperature and with a scan rate 5/min. The UV-VIS. absorption spectra were recorded on double beam spectrometer (Shimadzu model UV-3100) at room temperature for all the obtained glasses. The thickness of the samples is almost 1 mm and the wavelength range between 200 nm-800 nm. The resolution of the observed wave length is about ± 1 nm. The FT-IR spectra of the glasses were recorded at room temperature on JASCO-4200 model spectrometer. The KBr pellet technique was used and spectra were recorded in the range 400cm^{-1}-4000 cm^{-1} with wavelength resolution 2cm^{-1}. The Raman spectra was recorded on spectrometer with a resolution of 2cm^{-1} by using diode laser for excitation.

3. Results and Discussions

3.1 The XRD Analysis (X-ray diffraction)

X-ray diffraction spectrograms were recorded and there was no sharp peaks found. The absence of sharp crystalline peaks and presence of humps reflects the amorphous nature of the present glasses as shown in the **Fig.1**. The broad humps also found in the spectra, which is the characteristic nature of short range order or absence of crystalline nature. The characteristic broad humps were appeared in the spectra near 26-30 degree Bragg's angle.
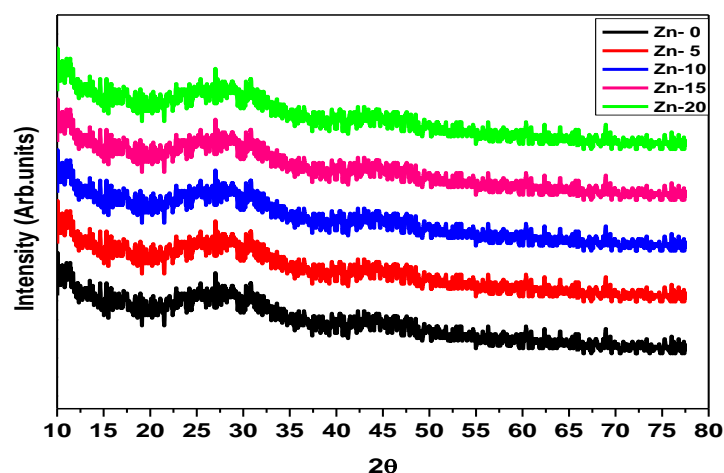
Fig.1. XRD patterns of ZnO incorporatedCaO-Sb$_2$O$_3$-B$_2$O$_3$ glasses

3.2 Density based studies

As demonstrated in the **Fig.2**, the experimental density measurements for the glasses revealed a linear increase from 2.72±0.01 gcm^{-3} to 3.26±0.01 gcm^{-3}. The greater molecular weight of ZnO (81.38 g.mol^{-1}) in comparison to the glass former B$_2$O$_3$ (69.61 g.mol^{-1}) may be the cause of the increasing trends in density values [**14**]. With a crystal density of 2.46 g.cm^{-3} for B$_2$O$_3$, the observed trends might potentially be explained. In the borate glass networks, the molar volume exhibits exactly opposite behavior to the density and is purely reliant on density [**15**].

The similar alterations in the behavior of molar volume were also discovered for the current study. Molar volume can be derived from the molecular weight and it decreased in the current investigation from 138.09 g.mol^{-1} to 129.63 g.mol^{-1}. The molar volumes (V$_m$) for the glasses ranged evenly from 50.76 cm^{-3}mol^{-1} to 39.76 cm^{-3}mol^{-1}. The density and oxygen content of amorphous materials determine the OPD. It fluctuated between 55.15 gatm.1^{-1} and 60.35 g.atm.1^{-1}, when the ZnO modifier component was added. This trend might be caused by an increase in the amount of collected oxygen ions in the glass domain as ZnO concentration rises [**16**]. **Table.1** provided the measured and computed physical variables that were independent and density dependent.
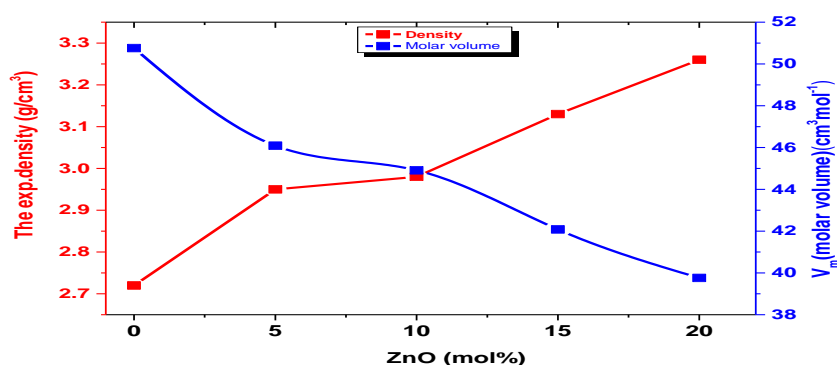

Fig.2. Density and molar volume of ZnO incorporated CaO-Sb$_2$O$_3$-B$_2$O$_3$ glasses

3.3 Ultraviolet visible spectra

Tauc plots provide important details regarding the direct (E_{direct}) and indirect (E_{ind}) band gap energies of several materials, including ferrites and glasses. Indirect band gaps work better for glassy materials than direct band gaps. For a direct band gap, the value of n is 0.5, and for an indirect band gap, it is 2. In the present investigation, the ZnO content increased and with respect to this, the cut- off wavelength increased from 298nm to 378 nm, as shown in **Fig.3**. **Table.1** provided the measured and computed physical variables that were independent and density dependent. The observed shift of cut- off wavelength towards the longer wavelength side could be explained by the creation of Non-Bridging Oxygens observed with increasing ZnO concentration. The pure sample with zero ZnO concentration has the lowest cut off wavelength value. ZnO and CaO, two network modifiers, perform the task of producing the maximum value of cut-off wavelength. There is an evidence that adding ZnO results in NBOs, and that is the quantity of NBOs rises as ZnO content [**17**].

The structural arrangement and composition of the host matrix are correlated with the energy gap. ZnO concentration increases cause the development of BO_3 units from BO_4 units, which raises the refractive index and decreases the bandgap energy. The lowest bandgap was 3.23eV for ZnO-0. The indirect E_{opt} values decreased from 3.90 eV to 3.23 eV when the ZnO concentration increased as shown in **Fig.4.** The **Fig.5** illustrates how the addition ZnO percentage affected the direct energy band gap of the present glasses, which varied between – 3.97eV to 3.32eV.

Table.1. The variations in the physical & optical parameters of ZnO incorporated CaO-Sb_2O_3-B_2O_3 glasses

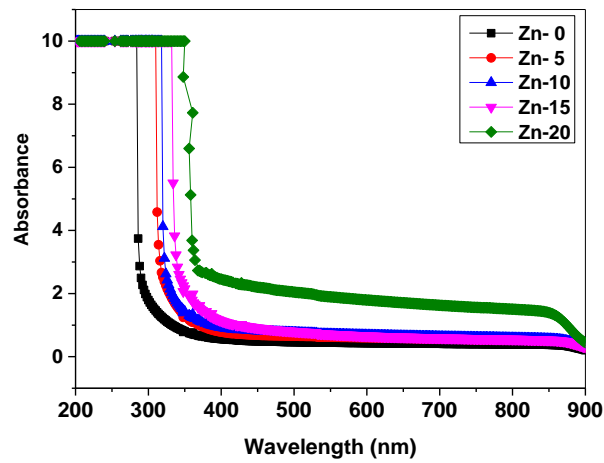| Parameter	Sample Code				
	Pure	**Zn-5**	**Zn-10**	**Zn-15**	**Zn-20**
Density (g.cm^{-3})(±0.01)	2.72	2.95	2.98	3.13	3.26
Molar mass (g.mol^{-1})	138.09	135.96	133.86	131.75	129.63
Molar volume (cm^{-3}.mol^{-1}) (±0.01)	50.76	46.09	44.91	42.08	39.76
OPD (g.atm.1^{-1}) (±0.15)	55.15	57.57	58.82	59.39	60.35
Cut off wavelength (nm) (±1nm)	296	312	324	361	374
Indirect energy band gap (±0.01eV)	3.90	3.76	3.63	3.41	3.23
Direct energy band gap(±0.01eV)	3.97	3.84	3.69	3.47	3.32
Urbach edge (±0.01eV)	0.65	0.73	0.78	0.83	0.90
Index of Refraction(±0.01)	2.12	2.15	2.19	2.22	2.30
Dielectric constant	4.49	4.62	4.79	4.92	5.29
Reflection loss	0.537	0.546	0.558	0.566	0.588
Molar refraction (cm^3/mol)	25.14	24.53	23.66	22.57	22.31
Electronic polarizability (10^{-24}cm^{-3})	8.34	8.64	8.72	9.02	9.28

Fig.3. The variation of absorbance with wavelength in UV-Absorption spectra of ZnO added glass series
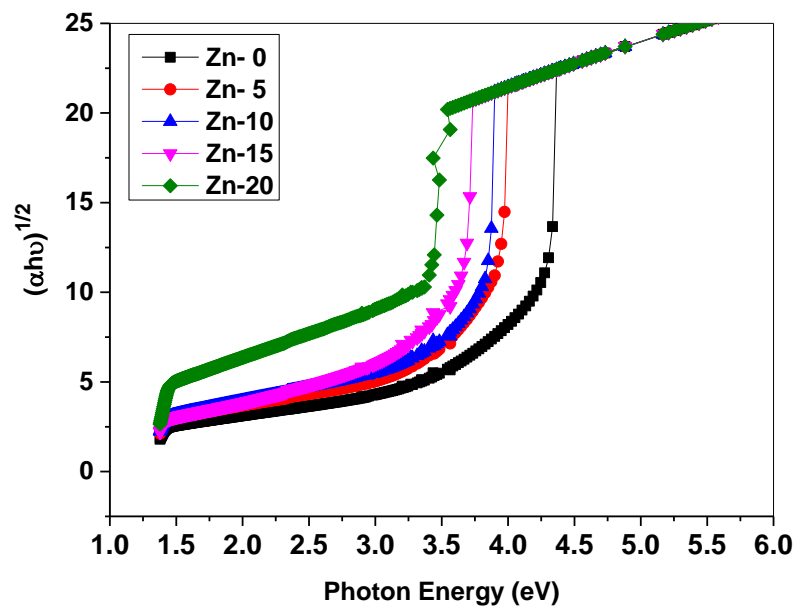

Fig.4 The indirect band gap calculation with UV-Absorption spectra of ZnO added glass series
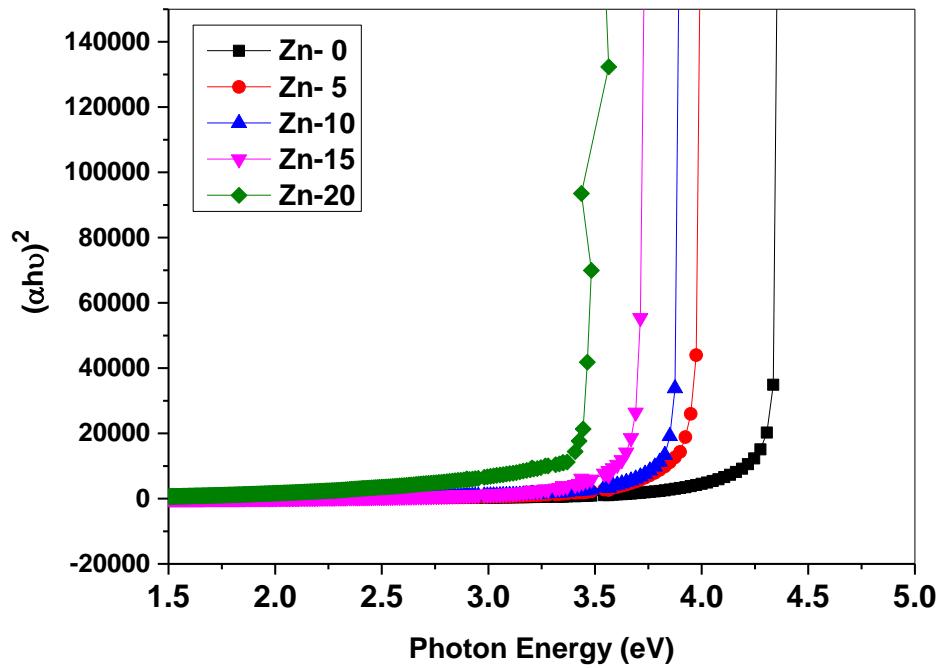
Fig.5. The direct band gap calculation with UV-Absorption spectra of ZnO added glass series
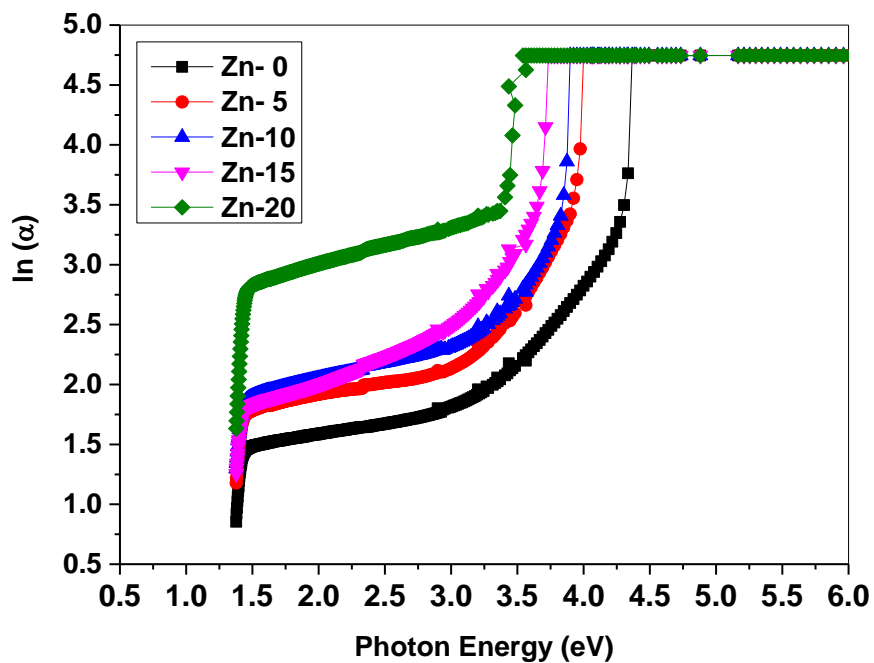

Fig.6. The Urbach energy plots of ZnO added glass series

In general, glassy materials are better suited for indirect band gap energies. The generation of negatively charged oxygen ions (NBOs) and the creation of metal-oxygen-glass former connections (Zn-O-B) are the causes of the growing trend of cut-off wavelength and reducing nature in band gap [**18**]. The previously indicated reason might also be attributed to the greater reflectivity index values of the examined ZnO system. As per the literature, an increase in ZnO concentration leads to a reduction in the values of the direct and indirect energy band gaps. Refractive index values for the existing glass system were also shown to be enhanced. The dielectric constant ranged from 4.49 to 5.29, and the reflection loss values increased from 0.537 to 0.588 with the modifier content. The molar refraction values of the ZnO glass series decreased from 25.14 to 22.31cm^3/mol, and the electronic polarizability values varied between 8.34 to 9.28 in the order of 10^{-24}cm^{-3} by adding ZnO, as shown in **Table.1**. The increase in cut-off wavelength, refractive index, and decrement in bandgap energy could be attributed to the formation of NBOs for all the examined glasses.

The disorder or flaws in the glass network are measured by the Urbach energy. More randomness or disorder in the matrix is confirmed by rising Urbach energy values [**19**]. The values were displayed in **Fig.6.** The determined values of the Urbach parameters are shown in **Table.1**. The glass system exhibited an increasing trend in Urbach energy, with values ranging from 0.65 to 0.90 eV. It's an indication of increasing disorder in the glass system, most likely brought on by structural alterations in the host glass as the concentration of network modifiers increases.

The behavioral variations in bandgap energy and refractive index as a function of ZnO modifier content have been discussed here. It is clear that the refractive index increases and the indirect wavelength decreases when the ZnO concentration rises. The behavior described above can be interpreted in terms of generation of NBOs [**20**]. **Table.1** represents all the measured and assessed optical parameters as well as the density-dependent physical characteristics of ZnO incorporated glass series.
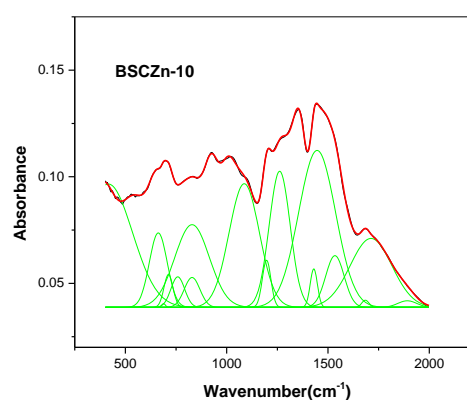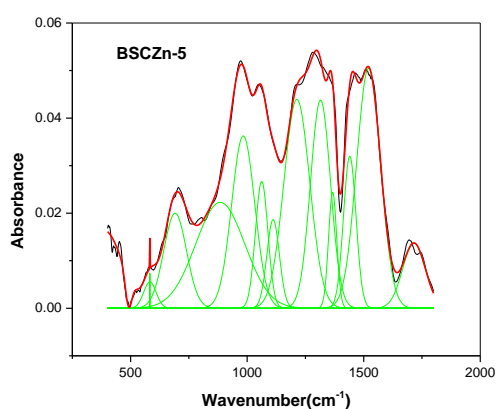
3.4 FTIR spectra

The composition system of the BSC-Zn glass series shows a fixed percentage of 10 for both Sb-O and Ca-O, a decrease in B$_2$O$_3$ molar concentration from 80% to 20%, and an increase in Zn-O molar percentage from 0% to 20% with a 5% increment in molar ratio. **Fig.7** shows the BSC-Zn glass series' FTIR spectra. Within this composition spectrum, the band positions of the BSC-Zn lass series were identified as follows: 395–415 cm^{-1}, 515–530 cm^{-1}, 696–725 cm^{-1}, 952-974 cm^{-1}, 1055-1079 cm^{-1},1209-1216 cm^{-1},1355-1360 cm^{-1}, 1446-1460 cm^{-1}, and 2800–2904 cm^{-1}[**21-23**].

Glass samples BSC-Zn were measured at room temperature using an FTIR spectrophotometer with a 400–4000 cm^{-1} measuring range [**24**]. Around 400cm^{-1} wavenumber regions particularly 395 to 415 cm^{-1} corresponds to the stretching vibrations of Zn-O linkage in tetrahedral linkage. At 696 to 725 cm^{-1} wavenumber domain corresponds to the bending vibration of B-O-B structural linkage. At 820 to 830 cm^{-1} wavenumber domain FTIR band attributed to the diborate linkage structure of B-O-B unit [**25, 26**]. Other FTIR

band appeared at 1025 to 1040 cm^{-1} wavenumber region related to the stretching vibration of penta borate structural unit. Broad and high absorbance band appeared at 1274-1285 cm^{-1} wavenumber domain corresponds to the asymmetric stretching vibrations of B-O linkage in BO$_3$ trigonal structure [27-29]. Around 1355 cm^{-1} region another peak was detected indicates the pyro borate structure in B-O linkage. At 1445-1455 cm^{-1} wavenumber domain corresponds to the symmetric stretching vibrations of B-O linkage in BO$_3$ structural unit [30-32]. B-O-M band linkage like B-O-Sb linkage type band appeared at 975 cm^{-1} wavenumber regions. As doping Zn content in host Boron structural unit, the variation of absorption peaks was found due to different ionic radii of metal ions [33].

Table.2 FTIR band positions of (80-x) B$_2$O$_3$-10 Sb$_2$O$_3$-10CaO-xZnO Glass system.

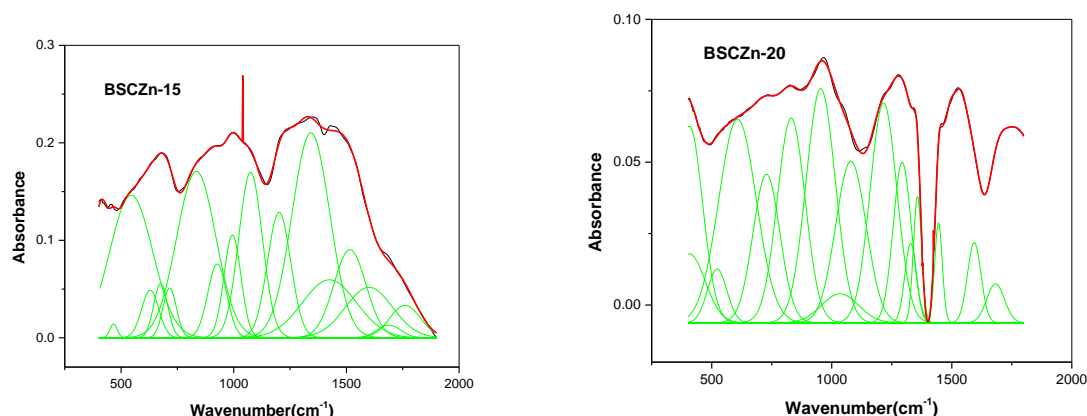| Characteristic bands	Assignment
395 to 415 cm^{-1}	Vibrations of Zn-O tetrahedral (ZnO$_4$).
696 to 725 cm^{-1}	Bending vibrations of B-O-B linkage
820 to 830 cm^{-1}	Bending vibrations of diborate structural unit
~975 cm^{-1}	B-O-M band linkage like B-O-Sb linkage
1025 to 1040cm^{-1}	Stretching vibrations of penta borate unit
1274-1285 cm^{-1}	Asymmetric stretching vibrations of B-O linkage in BO$_3$
~1355 cm^{-1}	Pyro borate structure in B-O linkage
1445-1455 cm^{-1}	Symmetric stretching vibrations of B-O linkage in BO$_3$ structural unit
2800-2904 cm^{-1}	H–O–H groups.

Fig.7 FTIR fittings of (80-x) B_2O_3-10 Sb_2O_3-10CaO-xZnO Glass system.

3.5.Raman spectral studies

BSC-Zn glass series structural composition was analysed by the room temperature Raman spectra wavenumber range from 200 to 2000 cm^{-1} and Raman spectrum drawn wavenumber against Raman intensity. **Fig.8** shows the Raman deconvoluted spectrum of the synthesized (80-x) B_2O_3-10Sb_2O_3-10CaO-xZnO (Where x = 0,5,10,15 and 20 mol%) glass system. The molar percentage of Zn-O content increases in the BSC-Zn glass series, whereas the concentration of B_2O_3 decreases and that of Sb_2O_3-CaO remains constant. These spectral graphs show Raman bands at wavenumber regions 265-280 cm^{-1}, 407-415cm^{-1},490-513cm^{-1}, 650-667 cm^{-1}, 708–718 cm^{-1}, 774–790 cm^{-1}, 978–983 cm^{-1}, 1130–1138 cm^{-1}, and 1340–1352 cm^{-1}[34-36].

The bending vibrations of the Zn-O structural unit are what gave the appearance of the band at 265-280 cm^{-1}. The isolated structure of the diborate ring is responsible for the Raman band at 407-415 cm^{-1}. This glass system contains a different kind of diborate ring structure that emerges at 490-513 cm^{-1}. An additional Raman band peak location was observed at 650-667 cm^{-1}, which is associated with the symmetric stretching vibrations of the borate group, specifically meta borate. The high intensity band at 708-718 cm^{-1} wavenumber area correlates to the stretching vibrations of the B-O-Sb structural unit. In the wavenumber range band associated with the boroxol ring unit, at 774-790 cm^{-1}[37, 38].
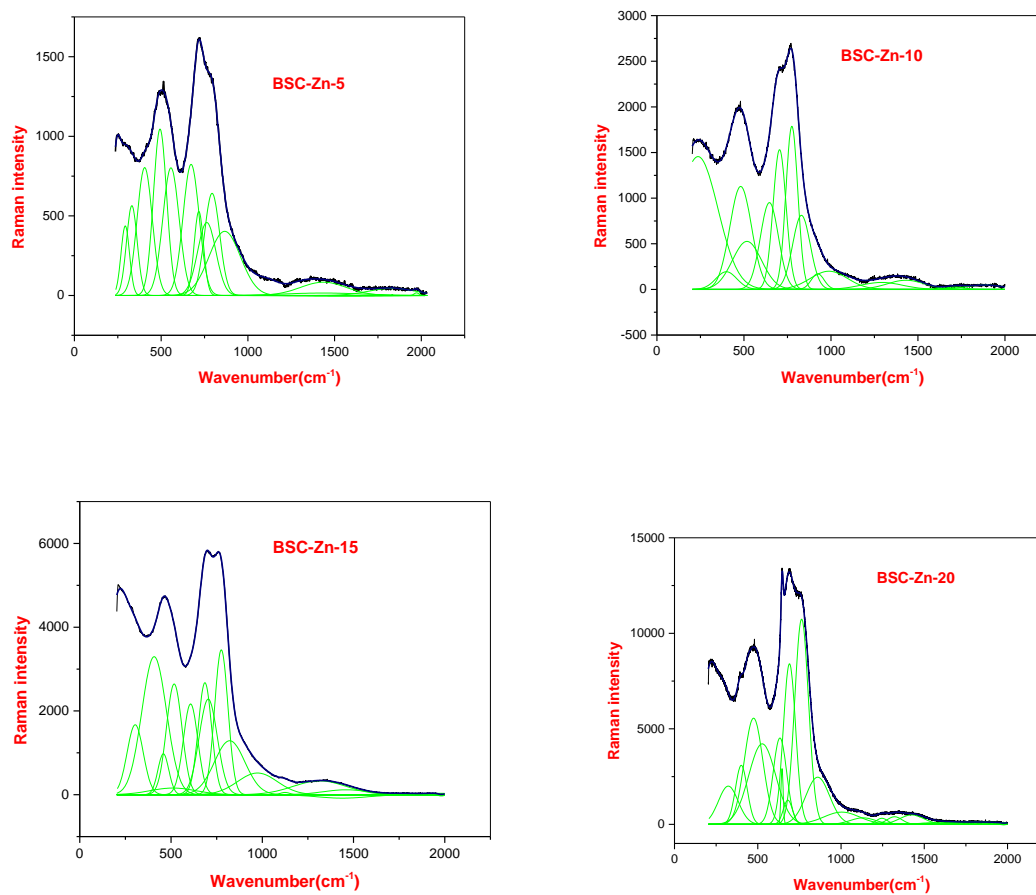
Rajesh Alukucha/ Afr.J.Bio.Sc. 6(8) (2024)

Fig.8. Raman deconvoluted spectrums of (80-x) B_2O_3-10Sb_2O_3-10CaO-xZnO glass system

The ortho borate structural unit's bending vibrations are responsible for the wavenumber range at the Raman peak, which is 978-983 cm^{-1}. The Raman band at 1130–1138 cm^{-1} is associated with the structural unit of the diborate ring. In addition to the bending vibrations of the chain structure, there is another Raman peak at 1340-1352 cm^{-1} that is associated with the meta borate ring [**39-42**].

Table.3. Raman band positions of (80-x)B_2O_3-10Sb_2O_3-10CaO-xZnO glass series

Characteristic bands	Assignment
265–280 cm^{-1}	Zn-O linkage bending vibrations
407–415 cm^{-1}	Isolate structure of diborate ring
490–513 cm^{-1}	Diborates unit
650-667 cm^{-1}	Meta borate symmetrical structural unit
708–718 cm^{-1}	B-O-Sb stretching vibrations

Rajesh Alukucha/ Afr.J.Bio.Sc. 6(8) (2024)

774–790 cm^{-1}	Boroxol ring unit
978–983 cm^{-1}	Ortho borate
1130–1138 cm^{-1}	Structural unit if di-borate group
1340–1352 cm^{-1}	Bending vibrations of meta borate chain ring structure

3.6 Conclusions

The selected glass composition $(80-x)B_2O_3-10Sb_2O_3-10CaO-xZnO$ with different x values were fabricated through rapid melt quench route. The non-crystalline nature of the glasses is determined by XRD analysis in which broad humps were presented. The density of the studied glasses increased as a function of ZnO molar content. From the optical analysis, cut-off wavelength increased: indirect and direct band gap energies decreased: Urbach energy increased. The variation of optical parameters occur because of the non-bridging oxygens. The FTIR spectra revealed the presence of M-O bonds along with peak shifting with the incorporation of ZnO. The Raman spectra is evident for different vibrations of molecules in localized structured glasses. The highest refractive index of the studied glasses make them suitable for NLO applications.

3.7 Acknowledgements

References

[1]. Ardiansyah Ardiansyah, Heryanto Heryanto, Bidayatul Armynah, Hassan Salah, Abdelmoneim Sulieman, David A. Bradley, Dahlang Tahir, Radiation Phy.Chem.,210 (2023) 111059, https://doi.org/10.1016/j.radphyschem.2023.111059.

[2]. Hasan Eskalen, Yusuf Kavun, Süleyman Kerli, Selami Eken, Opt. Mater. 105 (2020) 109871, https://doi.org/10.1016/j.optmat.2020.109871.

[3]. Rajat Ramteke, Kalpana Kumari, Soumalya Bhattacharya, M.R. Rahman, J. Alloys and Compounds,811 (2019) 151876, https://doi.org/10.1016/j.jallcom.2019.151876.

[4]. A.R. Ghazy, B.M. Elmowafy, A.M. Abdelghany, T.M. Meaz, R. Ghazy, R.M. Ramadan Scientific Reports, 13 (1 13) (2023), pp. 1-12, 10.1038/s41598-023-34458-4.

[5]. S.M. Elkatlawy, A.M. Abdel-Ghany, I.S. Yahia, H.A.A. El-Ghany, H.M. Gomaa, Boletín de La Sociedad Española de Cerámica y Vidrio, 61 (2022), pp. 733-744

[6]. Singkiburin, N. Srisittipokakun, J. Kaewkhao, *J. Phys.: Conf. Ser.* (2013) 012001.

[7]. Jun Li, Yin Zhang, Shangjiu Nian, Zhenning Wu, Weijing Cao, Nianying Zhou, Danian Wang, Applied Physics A 123 (2017) 205.

[8]. H.M.H. Zakaly, N.A.M. Alsaif, M.S. Shams, A.M. El‑Refaey, R.A. Elsad, M.S. Sadeq, · Y.S. Rammah, Optical and Quantum Electronics 55 (2023) 365

[9]. X. Fang, C. S. Ray, A. Mogus-Milankovic, D.E. Day, (2001). J. Non-Cryst. Solids 283 (2001) 162–172.

[10]. A.A. Kutub, K.A. Maghrab, C.A. Hoagarth,J. Mater. Sci., 22 (1987), pp. 2199-2202, 10.1007/BF01132960

[11]. S. Cetinkaya Colak, I. Akyuz, F. Atay, J. Non-Cryst. Solids, 432 (2016), pp. 406-412, 10.1016/j.jnoncrysol.2015.10.040

[12]. Vinoda Rani M., Naresh Pallati, Ravi Kumar Vuradi, Sadananda Chary A. Narender Reddy S., Journal of Non-Crystalline Solids,629 (2024) 122862, https://doi.org/10.1016/j.jnoncrysol.2024.122862.

[13]. Pallati Naresh, Boora Srinivas, D. Sreenivasu, D. Ravikumar, Gandla Nataraju, P. Sunitha Manjari, Gangadhar Talari, J. Laxman Naik, K. Siva Kumar,Journal of Non-Crystalline Solids,589(2022)121642, https://doi.org/10.1016/j.jnoncrysol.2022.121642.

[14]. Pallati Naresh, N. Narsimlu, Ch. Srinivas, Md. Shareefuddin, K. Siva Kumar, *J. Non. Cryst. Solids*.549 (2020) 120361.

[15]. P. Naresh, B. Kavitha, H. K. Inamdar, D. Srinivasu, N. Narsimlu, Ch. Srinivas, V. Sathe, K. Siva Kumar, *J.Non.Cryst.Solids*.514 (2019)35-45.

[16]. Shaik Amer Ahmed, Shaik Rajiya, M. A. Samee, Shaik Kareem Ahmmad, Kaleem Ahmed Jaleeli, J.Inorg.Organometallic Polym. Mater (2022) 32:941–953, https://doi.org/10.1007/s10904-021-02183-y

[17]. Pallati Naresh, J. Mol. Struct. 1213 (2020) 128184.

[18]. Navaneetha Pujari, Kalyani Birampally, Avula Edukondalu, C.P.Vardhani, *J. Phy. Chem. Solid*.148 (2021) 109627.

[19]. Vinoda Rani M., Naresh Pallati, Ravi Kumar Vuradi, Sadananda Chary A, Narender Reddy S., *J. Non. Cryst. Solids*, 629 (2024) 122862.

[20]. G. Lakshminarayana, Kawa M. Kaky, S.O. Baki, A. Lira, Priyanka Nayar,I.V. Kityk, M.A. Mahdi, J. Alloys Compd. 690 (2017) 799-816.

[21]. A. Saidu, H. Wagiran, M.A. Saeed, Y.S.M. Alajerami, Opt Spectrosc 117 (2014) 396–400. https://doi.org/10.1134/S0030400X14090239.

[22]. A.A. Abul-Magd, H.Y. Morshidy, A.M. Abdel-Ghany, Opt Mater (Amst) 109 (2020) 110301. https://doi.org/10.1016/J.OPTMAT.2020.110301.

[23]. B. Sumalatha, I. Omkaram, T. Rajavardhana Rao, C. Linga Raju, , Physica B Condens Matter 411 (2013) 99–105. https://doi.org/10.1016/J.PHYSB.2012.11.021.

[24]. M. Farouk, K. Abdallauh, M. Attallah, Z.M.A. El-Fattah, J Non Cryst Solids 523 (2019) 119607. https://doi.org/10.1016/J.JNONCRYSOL.2019.119607.

[25]. B. Sumalatha, I. Omkaram, T.R. Rao, C.L. Raju, J Non Cryst Solids 357 (2011) 3143–3152. https://doi.org/10.1016/J.JNONCRYSOL.2011.05.005.

[26]. B. Shanmugavelu, V. V. Ravi Kanth Kumar, Solid State Sci 20 (2013) 59–64. https://doi.org/10.1016/J.SOLIDSTATESCIENCES.2013.03.008.

[27]. R. Stefan, E. Culea, P. Pascuta, J Non Cryst Solids 358 (2012) 839–846. https://doi.org/10.1016/J.JNONCRYSOL.2011.12.079.

[28]. M.S. Gaafar, N.S.A. El-Aal, O.W. Gerges, G. El-Amir, J Alloys Compd 475 (2009) 535–542. https://doi.org/10.1016/J.JALLCOM.2008.07.114.

[29]. A.A. El-Daly, M.A. Abdo, H.A. Bakr, M.S. Sadeq, Ceram Int 47 (2021) 31470–31475. https://doi.org/10.1016/J.CERAMINT.2021.08.024.

[30]. S. Cetinkaya Colak, I. Akyuz, F. Atay, J Non Cryst Solids 432 (2016) 406–412. https://doi.org/10.1016/J.JNONCRYSOL.2015.10.040.

[31]. R. Ramteke, K. Kumari, S. Bhattacharya, M.R. Rahman, J Alloys Compd 811 (2019) 151876. https://doi.org/10.1016/J.JALLCOM.2019.151876.

[32]. M. Farouk, A. Samir, A. Ibrahim, M.A. Farag, A. Solieman, Applied Physics A 126 (2020) 696. https://doi.org/10.1007/s00339-020-03890-y.

[33]. N.A.M. Alsaif, H.I. Alrebdi, Y.S. Rammah, M.S. Shams, Journal of Materials Science: Materials in Electronics 34 (2023) 1914. https://doi.org/10.1007/s10854-023-11277-x.

[34]. R. Ramteke, K. Kumari, S. Bhattacharya, M.R. Rahman, J Alloys Compd 811 (2019) 151876. https://doi.org/10.1016/J.JALLCOM.2019.151876.

[35]. .A. Osipov, L.M. Osipova, B. Hruška, A.A. Osipov, M. Liška, Vib Spectrosc 103 (2019) 102921. https://doi.org/10.1016/J.VIBSPEC.2019.05.003.

[36]. M. Farouk, A. Samir, A. Ibrahim, M.A. Farag, A. Solieman, Raman, Applied Physics A 126 (2020) 696. https://doi.org/10.1007/s00339-020-03890-y.

[37]. A.M. Zahra, C.Y. Zahra, B. Piriou, DSC and Raman studies of lead borate and lead silicate glasses, J Non Cryst Solids 155 (1993) 45–55. https://doi.org/10.1016/0022-3093 (93) 90470-I.

[38]. A.K.Yadav,P.Singh,RSC.Adv,5(2015)67583–67609. https://doi.org/10.1039/C5RA13043C.

[39]. G. Sangeetha, K. Chandra Sekhar, M. Narasimha Chary, Md. Shareefuddin, Optik (Stuttg) 259 (2022) 168952. https://doi.org/10.1016/j.ijleo.2022.168952.

[40]. M.N. Svenson, M. Guerette, L. Huang, M.M. Smedskjaer, J Non Cryst Solids 443 (2016) 130–135. https://doi.org/10.1016/j.jnoncrysol.2016.04.023.

[41]. B. Łagowska, I. Wacławska, M. Sitarz, M. Szumera, J Mol Struct 1171 (2018) 110–116. https://doi.org/10.1016/j.molstruc.2018.05.085.

[42]. Jagram anterbedy, Naresh Pallati, Aravind Seema, Rajesh Alukucha, Gangadhar Thalari, *ECS J. Solid State Sci. Technol.* 13(2024) 043012

[43].